J. Agr. Sci. Tech. (2021) Vol. 23(1): ??-??

Dynamics Analysis of Obstacle Avoidance of Tomato Side Branch Pruning Robotic Arm

F. Yin[1], Y. Shen[1, 2], Y. Chen[1], C. Zhang[2], and M. Wu[1,*]

ABSTRACT

The side branches in tomato plants have a great impact on tomato yield and fruit quality and the pruning work is now basically done manually, which has high labor intensity and high-risk factor. The elevated cultivation of tomatoes was taken as the objective of this research and 6 degrees of freedom P-R-R-R-R-R tomato side branch pruning robotic arm was proposed. The dynamic simulation of the robotic arm in the obstacle environment was completed by ADAMS. Simulation results showed the angular velocity and angular acceleration curves of each joint. A trajectory planning method combining Cartesian space and joint space was proposed to ensure that the robotic arm can avoid obstacles while effectively reducing the impact during operation.

Keywords: ADAMS, Dynamic simulation, Elevated tomato, Trajectory planning.

[DOR: 20.1001.1.16807073.2021.23.1.16.9]

INTRODUCTION

The planting areas of tomato worldwide have exceeded 2,000 km^2 (Silva *et al.* 2017), and the market demand for tomatoes and related products is huge. On the other hand, due to the strong growth ability of side branches in tomato plants, excessive auxiliaries absorb nutrients and affect the development of main branches, which have a greater impact on tomato yield and fruit quality (Kanyomeka, and Shivute, 2005; Maboko, and Du Plooy, 2018; Ara, *et al.* 2007, Dursun *et al.* 2019). At present, the side branch pruning of tomatoes is still basically done by hand, which is labor-intensive. In addition, in order to improve planting efficiency and space utilization, more and more planting bases have begun to adopt elevated cultivation methods, which often require laborers to climb ladders. The use of ladder itself has a high-risk factor, high labor intensity, and pruning efficiency and pruning quality is affected.

At present, the research work on the side branch pruning is still relatively rare (He, Schupp 2018; Huang, *et al.* 2016; Vasconez, *et al.*; Sabanci, K. and Aydin, C. 2018). In 2011, Ueki *et al*., improved the third generation of lightweight climbing pruning robot and completed the indoor simulation experiment. The robot consists of 4-foot wheel moving mechanism and chain saw trimming actuator. When the target side branch is positioned, the robot rotates at a low speed in the circumferential direction, and the chain saw rotates to complete the side branch trimming. (Fu *et al*. 2015) proposed a climbing type fast-growing forest pruning robot in 2015 that can accommodate a trunk diameter range of 150 to 350 mm. The robot was combined with the clamping device and the climbing device, and the turntable mechanism drives the circular saw to rotate in the circumferential direction to complete the pruning work. In addition, (Soni *et al*. 2010) proposed a betel tree pruning

[1] College of Mechanical and Electrical Engineering, Wenzhou University, Wenzhou 325035, P. R. China.
[2] Institute of Agricultural Equipment, Zhejiang Academy of Agricultural Science, Hangzhou 310021, P. R. China.
[*] Corresponding author; e-mail: wmg7810@wzu.edu.cn

robot that uses two methods of attaching the surface of the trunk to climb and cut hard side branches with high hardness materials. Some scholars have carried out research on the side branch pruning of vines, such as the pruning robot jointly developed by the Gifu University in Japan (Kawasaki *et al.* 2008; Ishigure *et al.* 2013), the grape pruning robot system developed by the University of Canterbury in 2017 (Botterill, *et al.* 2017), and other branch pruning machines (Peña, *et al.* 2018; Zhu *et al.* 2018; Gui *et al.* 2018; Khoshnevisan *et al.* 2015; Lau *et al.* 2013), but such robots cannot be used to prune high-environment and soft-spotted tomato side branches.

There are many types of harvesting robots, such as automatic harvesting robot for cucumber (Henten *et al.* 2003), cherry (Tanigaki *et al.* 2008), tomato (Monta *et al.* 1998), strawberry (Hayashi *et al.* 2010), and sweet-pepper (Bac *et al.* 2016). In 2014, Shigehiko *et al.*; Hayashi *et al*. 2014, designed a 7-DOF greenhouse strawberry picking robot installed on a mobile platform which was capable of moving between ridges. In 2013, (Chiu *et al*. 2013) developed a greenhouse tomato picking system with a 4-finger gripper on the end effector.

The fruit sags naturally due to its own weight, and the stalk attached to it is therefore at a small angle to the direction of gravity, making the stalk separation relatively easy. However, the side branches of tomato are light, and there is no obvious growth or distribution patten for that. Therefore, compared with the harvesting robots, side branch pruning has higher requirements for the flexibility of the robot, and the actuator structure should be as light as possible.

In this study, combined with the action flexibility of tomato side-branch pruning and the lightness requirements of the actuator structure, the overall structure scheme of the side branch pruning robotic arm was proposed. At the same time, with the aim of no obvious impact in the movement process, the dynamic simulation of the robotic arm in the obstacle environment was completed by the software ADAMS. Simulation results show the angular velocity and angular acceleration curves of each joint. A trajectory planning method combining Cartesian space and joint space was proposed to ensure that the robotic arm can avoid obstacles while effectively reducing the impact during operation.

MATERIALS AND METHODS

Model Description

Elevated Tomato Cultivation Environment

The cultivation method of the tomato planting base is shown in Figure 1-a, where the overhead slings are arranged in a three-dimensional suspension and tomatoes are planted along the ridges. The minimum growth height of tomato vines is 0.5 m, the highest is 3.5 m, the ridge spacing is 1.5 m, and the ridge width is 0.2 m. The distribution space of the tomato side branches was contained in the tomato growth space, and the upper limit of the horizontal direction was the ridge width. Therefore, the horizontal width of the side branch distribution plane was 0.2 m. It can be seen from the above view that the main plane of the tomato side branch spatial distribution, that is, the target working plane of the trimming robotic arm, was a rectangular area with a width B= 200 mm, a height L= 3,000 mm, and a centroid horizontal interval A= 1,500 mm, as shown in Figure 1-b. Because the distribution plane of tomato side branches was slender and the width-to-height ratio was only 1/20, the influence of the overall freedom of the robotic arm on the flexibility of the robot's end in horizontal movement should be considered in the design process.

Structure of Tomato Side Branch Pruning Robotic Arm

In order to realize the tomato side branch pruning function, the robot end-effector

[DOR: 20.1001.1.16807073.2021.23.1.16.9]

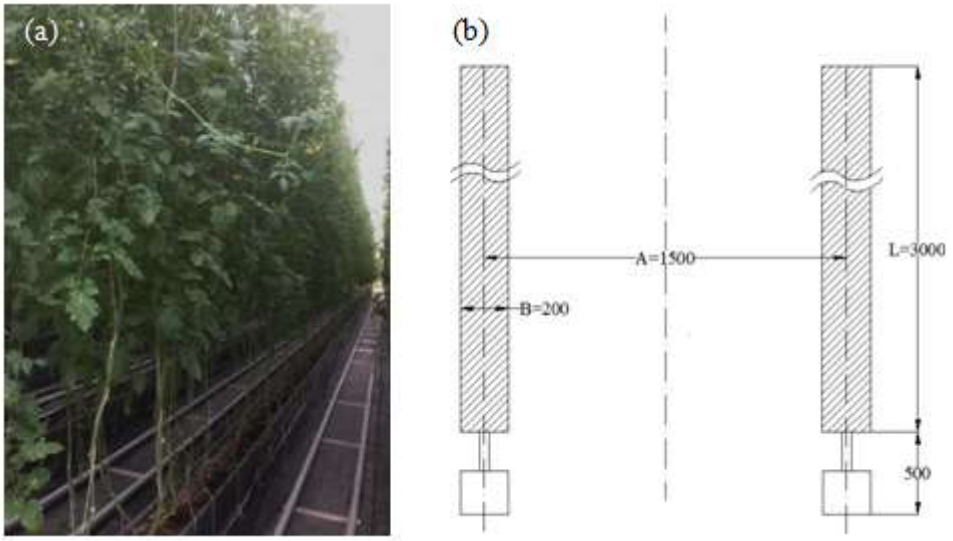

Figure 1. (**a**) Elevated tomato cultivation mode, and (**b**) Target working plane of tomato collateral pruning manipulator.

should be able to approach the side branch at any angle, and the robotic arm should have at least one set of big and small arms unit. In addition, the end-effector itself has a certain volume, in order to prevent it from touching other plants before reaching the designated position. It should also have a rotating obstacle-avoiding joint along the axis of the end-effector itself. Finally, considering the versatility replaceable of end-effector, the robotic arm needs to have a wrist unit that can adjust the position of the end-effector and keep it horizontal at any time.

Above all, the tomato side branch pruning robotic arm should have a waist lift unit, waist rotation unit, big arm tilt unit, small arm swing unit, wrist horizontal adjustment unit, and axial obstacle avoidance joint unit, which will be a P-R-R-R-R-R type joint robotic arm with 6 Degrees Of Freedom (DOF). The overall kinematics diagram of the tomato side branch pruning robotic arm is shown in Figure 2-a, the two-degree-of-freedom mobile platform realizes the forward and backward movement along the track and the lateral movement on the ground.

The simulation diagram of the size parameter of the main working plane of the robotic arm is shown in Figure 2-c, which was stimulated by the graphic method to solve the main size of the rod length, swing angle, and lift range. The main working plane of the robotic arm was determined as follows:

(1) Take a rectangular area S_{ABCD} as the target space. The positions of the rectangular boundary points were A= (650, 0, 500), B= (850, 0, 500), and points C and D were respectively located at x= 850 and x= 650 on the projection line of the target area.

(2) When the swing angle of the big arm takes the maximum value, the arc *GH* is drawn by the radius of the small arm length and the range of swing angle. And the arc *IJ* is drawn when the swing angle of the big arm takes the minimum value.

(3) When the swing angle of the small arm takes the maximum value, the arc *GI* is drawn by the radius of the big arm length and the range of swing angle. And the arc *HJ* is drawn when the swing angle of the small arm takes the minimum value.

(4) When the small arm swing angle takes the maximum value, the center of arc *GI* is translated upward in the vertical direction by a suitable distance as a new center. Then, the arc *HI* is drawn by the radius of the big arm

[DOR: 20.1001.1.16807073.2021.23.1.16.9]

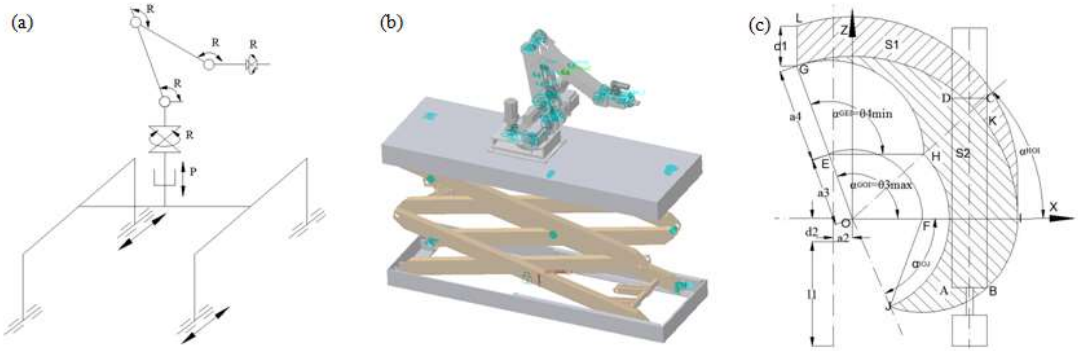

Figure 2. (**a**) Kinematics diagram of tomato side branch pruning robotic arm; (**b**) Virtual prototype model, and (**c**) Dimensional parameter simulation of tomato collateral pruning robotic arm.

length and the range of swing angle, and connects the line segment *LG*.

The MATLAB optimization function was used to find the optimal solution for each joint parameter. Finally, the size parameters of each joint variable obtained were as follows: Lift range d_1= 2 m, arm Length a_3= a_4= 0.420 m, swing angle of big arm θ_3= 0°~100°, swing angle of small arm θ_4= -131°~0°.

Dynamics Simulation of Obstacle Avoidance

General Point Drive Method

It is assumed that there is a main branch or tomato fruit between the straight path between section boundary point E and the target side branch point I, which is called the obstacle J. In order to avoid the physical damage caused by the direct collision to J, multi-segment stitching path *EKI* was considered to cross the obstacle J and achieve non-destructive pruning. The schematic diagram of the end-effector path *GEKI* in the main working plane is shown in Figure 3.

Taking the polyline path *GEKC* of upper half-plane as an example, the waist joint was rotated by 90° from the initial position in 3 seconds, so that the end-effector reached the new initial position G in the main working plane, the point G was close to the point E on the boundary of the target space after 1 second, so far the position adjustment was completed. Then, it rose vertically to point K in 2 seconds, and then took 4 seconds to reach the target position C point with the circular path *KC*, and the crossing of the obstacle J was completed. The total time taken from the initial position to the target position in the process was 3+1+2+4=10 seconds. The point drives of the arc path added at the end-effector point are shown as follows and the simulated arc polyline path *GEKC* is shown in Figure 4-a.

X axis:

IF(time-3:0,0,IF(time-4:STEP5(time,3,0,4,62.92196833),62.922,IF(time-6:STEP5(time,4,62.922,6,62.922),62.922,62.922+(200-200*cos((time-6)*PI/6)))))

Z axis:

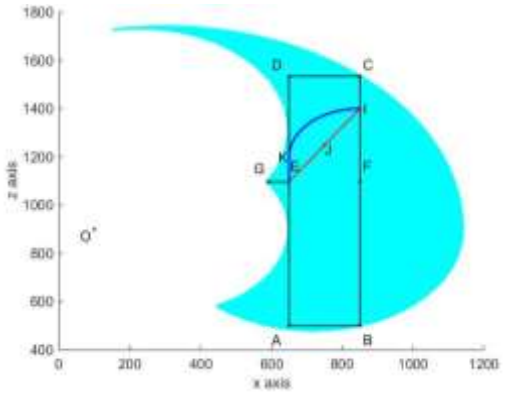

Figure 3. Schematic diagram of multi-segment path GEKI.

[DOR: 20.1001.1.16807073.2021.23.1.16.9]

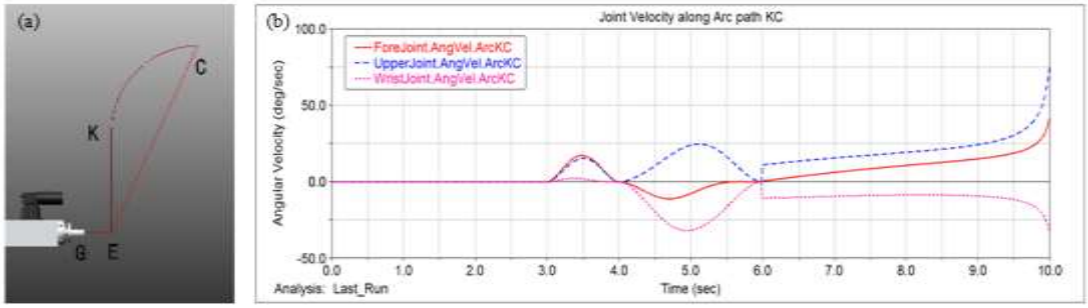

Figure 4. (**a**) The arc path KC, and (**b**) Angular velocity of each joint along arc path KC.

IF(time-3:0,0,IF(time-4:STEP5(time,3,0,4,0),0,IF(time-6:STEP5(time,4,0,6,232.6967351971),232.6967351971,232.6967351971+200*sin((time-6)*PI/6))))

Figure 4-b shows the angular velocity of each joint along the arc path *GEKC*. In the first 6 seconds, the endpoint was moved along the simple linear path GE and EK, and the fifth-order polynomial was used as the drive function, and the joint speed curve was smooth and continuous, the angular velocity was 0 when the motion stopped. The drive function after the 6th second was a plane circular path in the Cartesian space, while the first derivative of the drive function was not 0 at the 6th second, which means it had an initial velocity at that time. Thus, the paths EK, KC had only a continuous displacement curve at the joint point K, while the angular velocity curves of the small arm and the wrist joint were not continuous, resulting in obvious angular velocity of the joint and a greater impact at the 6th second. Moreover, at the 10th second of the end of the process, the angular velocities of the three parallel joints were not 0, resulting in another significant impact. These two impacts will have a certain degree of influence on the accuracy of the robotic arm and the quality of the movement.

Optimization of Drive Function

To ensure accurate and smooth pruning, the two impacts that existed in the 6th and 10th seconds should be eliminated. If the KC path was directly driven by the high-order polynomial drive function, which was equivalent to the joint space, trajectory planning finished between the two known coordinates in the target section *S*ABCD, it can ensure the smooth movement of the robotic arm during the last 4 seconds, but also made the movement path of the endpoint difficult to predict. In order to meet the requirements of obstacle avoidance work, the robotic arm needed to add path points frequently during the KC path and perform high-order polynomial interpolation, which makes this method much more computationally complex.

It can be considered the trajectory planning method combining Cartesian space and joint space, so the KC path will be divided into two, while the previous segment of the simulation takes into account both obstacle avoidance and smooth operation and the latter segment of the simulation uses the high-order polynomial drive function to interpolate, ensuring that the robotic arm can complete the obstacle avoidance action while reducing the amount of calculation and minimizing the impact.

For the velocity sudden change at the 6th second, the original circular movement drive function can be combined with the cycloidal motion law to construct a new drive function in the first half of the KC path. The form was the product of the displacement curve of the cycloidal motion characteristic and the circular path displacement expression. This has the characteristics that the first position

[DOR: 20.1001.1.16807073.2021.23.1.16.9]

E and last position C coordinates remain unchanged and the first derivative is continuous, which can ensure that the angular velocity curves of the driving functions of the two paths of EK and KC are continuous at the 6th second, so that the robotic arm can runs smoothly along the KC path. The modified end-effector point drive functions are shown as follows, and the path along the drive is shown in Figure 5-a as the pink polyline, and the simulation results are shown in Figures 5-b and -c.

X axis:

IF(time-3:0,0,IF(time-4:STEP5(time,3,0,4,62.92),62.922,IF(time-6:STEP5(time,4,62.922,6,62.922),62.9223,62.922+((time-6)/3-sin(2*PI*(time-6)/3)/(2*PI))*(200-200*cos((time-6)*PI/6)))))

Z axis:

IF(time-3:0,0,IF(time-4:STEP5(time,3,0,4,0),0,IF(time-6:STEP5(time,4,0,6,232.6967),232.6967,232.6967+((time-6)/3-sin(2*PI*(time-6)/3)/(2*PI))*200*sin((time-6)*PI/6))))

As shown in Figure 5-b, the angular velocity of the small arm and wrist joints after the improvement of the drive were no longer abrupt. If the cycloid motion characteristic displacement function was regarded as the coefficient of the circular path displacement drive function, the influence on the latter gradually disappeared with the gradual progress of the simulation. As shown in Figures 5-b and -c, when the simulation was almost ending, the speed and acceleration of the three parallel joints were gradually consistent with the results of the circular path KC. The acceleration of small arm was close to 500° s^{-2} at the 10th second, and the acceleration of the big arm and wrist joint were close to 250° s^{-2}.

In order to effectively reduce the angular acceleration of the three parallel joints, the 8th second was selected as the boundary point of the second half of the KC path for the fifth-order polynomial interpolation. The velocity and acceleration curves of the endpoint along the X-axis and the Z-axis were fitted with a spline function and output to the data unit. It was found that at the 8th second, the displacement of the endpoint along the X-axis was 92.2113 mm, and the velocity was 57.0573 mm s^{-1}, the acceleration was 66.4405 mm s^{-2}, and when the point C was reached, the displacement of

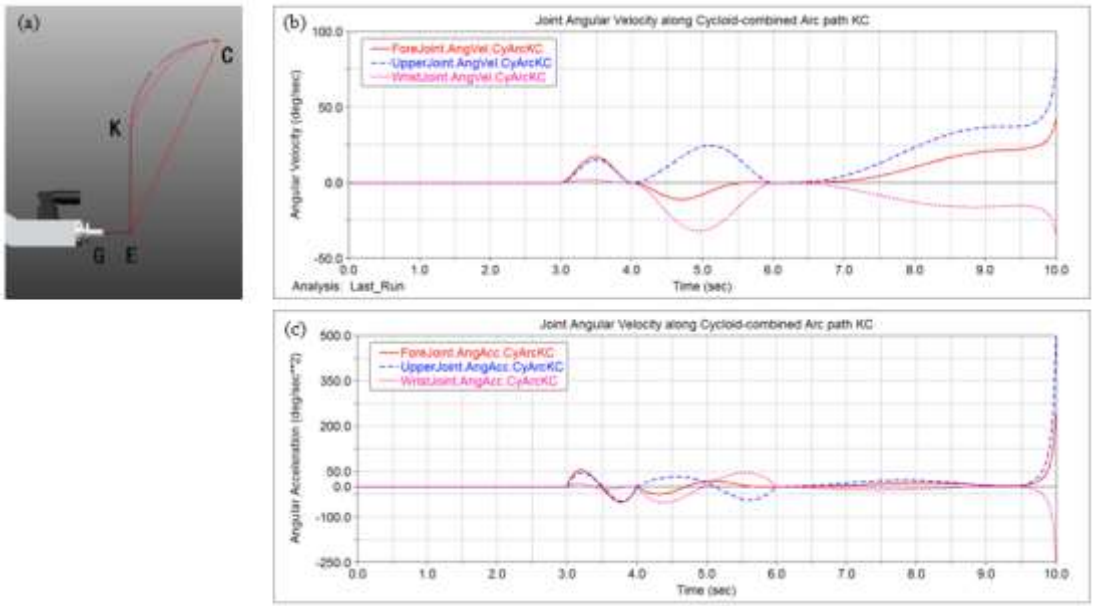

Figure 5. (**a**) The cycloid-combined arc path KC; (**b**) Angular velocity of each joint along arc path KC, and (**c**) Angular acceleration of each joint along arc path KC.

[DOR: 20.1001.1.16807073.2021.23.1.16.9]

the endpoint was 850-587.0780= 262.922 mm, and the speed and acceleration were both 0. Using the above two sets of data as boundary conditions, the fifth-order polynomial interpolation function of the second half of the KC path can be solved. In the same way, the drive function along the Z-axis from the 8th to the 10th second can be obtained. The final point drive function applied to the end-effector was obtained and the path along the drive is shown in the blue polyline of Figure 6-a.

X axis:

IF(time-3:0,0,IF(time-4:STEP5(time,3,0,4,62.922),62.922,IF(time-6:STEP5(time,4,62.922,6,62.922),62.922,IF(time-8:62.922+((time-6)/4-sin(2*PI*(time-6)/4)/(2*PI))*(200-200*cos((time-6)*PI/8)),92.2113,92.2113+57.0573*(time-8)+0.5*66.4405*(time-8)**2+77.972*(time-8)**3-78.0687*(time-8)**4+17.1575*(time-8)**5))))

Z axis:

IF(time-3:0,0,IF(time-4:STEP5(time,3,0,4,0),0,IF(time-6:STEP5(time,4,0,6,232.6967),232.6967,IF(time-8:232.6967+((time-6)/4-sin(2*PI*(time-6)/4)/(2*PI))*200*sin((time-6)*PI/8),303.4074,303.4074+98.4787*(time-8)+0.5*44.6316*(time-8)**2-19.580*(time-8)**3-5.993*(time-8)**4+2.9875*(time-8)**5))))

The spatial polyline path obtained by adding the corresponding drive to each joint as shown in Figure 6-b, and the simulation results of the angular velocity and angular acceleration of each joint are shown in Figures 6-c and -d. In the first 8 seconds, the angular velocity and angular acceleration of the three parallel joints were consistent with the simulation results of the first 8 seconds of the cycloidal arc KC, and during the 8th to 10th second, the angular velocity first increased and then decreased after the fifth-order polynomial and reached 0 at the 10th second. The angular acceleration curve was first increased, then decreased, then increased in reverse, and then decreased to 0. The angular velocity and angular acceleration curve of each joint was continuous without abrupt change, which can be considered as no impact during operation. The extremum of angular velocity and angular acceleration happened at 9.2

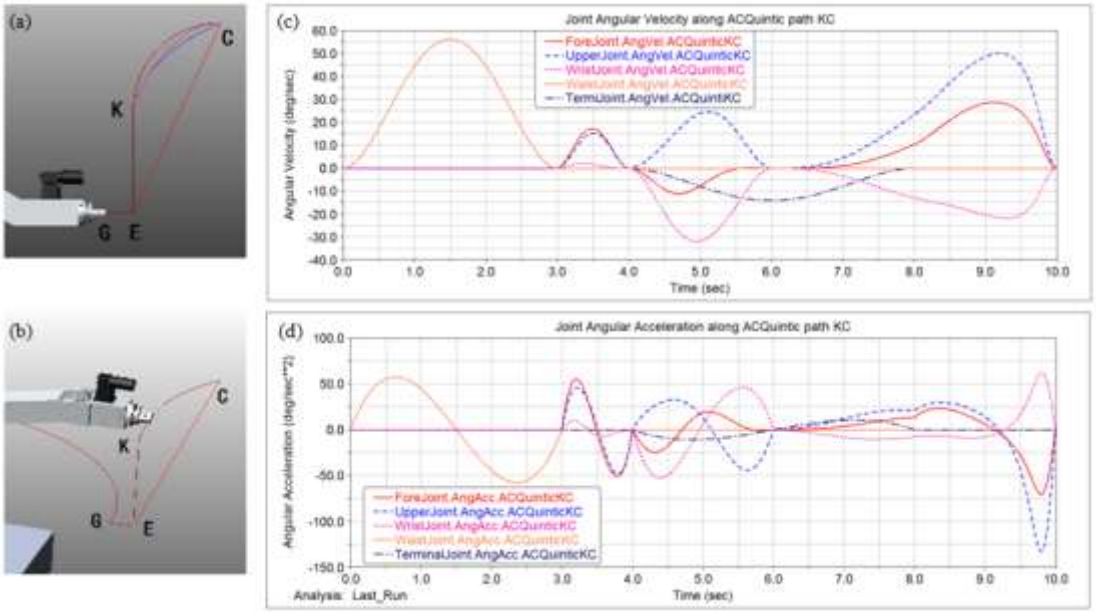

Figure 6. (a) The cycloid-combined plane arc path KC with fifth-order polynomials interpolation; (**b**) Multisegment line GEKC; (**c**) Angular velocity of each joint along arc path KC, and (**d**)Angular acceleration of each joint along arc path KC.

[DOR: 20.1001.1.16807073.2021.23.1.16.9]

seconds and 9.83 seconds, which were 50.17° s^{-1} and -130° s^{-2}, respectively.

CONCLUSIONS

A 6 DOF P-R-R-R-R-R tomato side branch pruning robotic arm was proposed. With the aim of no obvious impact in the movement process, the dynamic simulation of the robotic arm in the obstacle environment was completed by ADAMS. Simulation results showed the angular velocity and angular acceleration curves of each joint. A trajectory planning method combining Cartesian space and joint space was proposed to ensure that the robotic arm could avoid obstacles while effectively reducing the impact during operation. Finally, the extremum of angular velocity and angular acceleration happened at 9.2 seconds and 9.83 seconds, respectively, and were 50.17° s^{-1} and -130° s^{-2}, which can be considered as no impact during operation.

ACKNOWLEDGEMENTS

This paper is supported by the Laser and Photoelectric Intelligent Manufacturing Institute of Wenzhou University, Zhejiang Academy of Agricultural Science and the Key Research and Development Plan of Zhejiang. This research was funded by the Key Technology Research and Development Program of Zhejiang, grant number 2017C02018 and the Key Technology Research and Development Program of Zhejiang, grant number 2019C02019.

REFERENCES

1. Ara, N., Bashar, M. K. and Begum, S. 2007. Effect of Spacing and Stem Pruning on the Growth and Yield of Tomato. *Int. J. Sustain. Crop Prod.*, **2:** 35-39.
2. Bac, C. W., Roorda, T. and Reshef, R. 2016. Analysis of a Motion Planning Problem for Sweet-Pepper Harvesting in a Dense Obstacle Environment. *Biosyst. Eng.,* **146:** 85-97.
3. Botterill, T., Paulin, S. and Green, R. 2017. A Robot System for Pruning Grape Vines. *J. FIELD ROBOT,* **34:** 1100-1122.
4. Chiu, Y. C., Yang, P. Y. and Chen, S. 2013. Development of the End-Effector of a Picking Robot for Greenhouse-Grown Tomatoes. *Appl. Eng. Agric.* **29:** 1001-1009.
5. Dursun, A., Yildirim, E., Turan, M., Ekinci, M., Kul, R., and Parlakova Karagoz, F. 2019. Determination of the Effects of Bacterial Fertilizer on Yield and Growth Parameters of Tomato. *J. Agr. Sci. Tech.*, **21:** 1227-1234.
6. Fu, G. H., Liu, X. M. and Chen, Y. F. 2015. Fast-Growing Forest Pruning Robot Structure Design and Climbing Control. *Adv. Manuf.*, **3:** 166-172.
7. Gui, P., Tang, L. and Mukhopadhyay, S. 2018. A Novel Robotic Tree Climbing Mechanism with Anti-Falling Functionality for Tree Pruning. *J. Mech. Robot.*, **10:** 014502.
8. Hayashi, S., Yamamoto, S. and Saito, S. 2014. Field Operation of a Movable Strawberry-harvesting Robot using a Travel Platform. *JARQ-Jpn. Agr. Res. Q,* **48:** 307-316.
9. Hayashi, S., Shigematsu, K. and Yamamoto, S. 2010. Evaluation of a Strawberry-Harvesting Robot in a Field Test. *Biosyst. Eng.*, **105:**160-171.
10. He, L. and Schupp, J. 2018. Sensing and Automation in Pruning of Apple Trees: A Review. *Agronomy-Basel,* **8:** 211.
11. Henten, E. J. V., Tuijl, J. V. and Hemming, J. 2003. Field Test of an Autonomous Cucumber Picking Robot. *Biosyst. Eng.*, **86:** 305-313.
12. Huang, B., Shao, M. and Chen, W. 2016. Design and Research on End Effector of a Pruning Robot. *Int. J. Simul. Model.*, **17:** 1-5.
13. Ishigure, Y., Hirai, K. and Kawasaki, H. 2013. A Pruning Robot with a Power-Saving Chainsaw Drive. 2013 IEEE International Conference on Mechatronics and Automation, 4 August 2013, Takamatsu, Japan, ***IEEE:*** 1223-1228.
14. Kanyomeka, L. and Shivute, B. 2005. Influence of Pruning on Tomato Production under Controlled Environments. *Agricultura Tropica et Subtropica,* **38:** 79-83.

[DOR: 20.1001.1.16807073.2021.23.1.16.9]

15. Kawasaki, H., Murakami, S. and Kachi, H. 2008. Novel Climbing Method of Pruning Robot. *2008 SICE Annual Conference*, 20 Aug. 2008, Tokyo, Japan, ***IEEE:*** 160-163.
16. Khoshnevisan, B., Rafiee, S., Iqbal, J., Shamshirband, S., Omid, M., Badrul, A. N. and Abdul, W. A. 2015. A Comparative Study between Artificial Neural Networks and Adaptive Neuro-Fuzzy Inference Systems for Modeling Energy Consumption in Greenhouse Tomato Production: A Case Study in Isfahan Province. *J. Agr. Sci. Tech.*, **17:** 49-62.
17. Lau, S. C., Othman, W. and Bakar, E. A. 2013. Development of Slider-Crank Based Pole Climbing Robot. *IEEE International Conference on Control System, Computing and Engineering*, 29 November 2013, Mindeb, Malaysia, ***IEEE:*** 471-476.
18. Maboko, M. M. and Du Plooy, C. P. 2018. Response of Field-Grown Indeterminate Tomato to Plant Density and Stem Pruning on Yield. *Int. J. Veget. Sci.*, **24:** 612-621.
19. Monta, M., Kondo, N. and Ting, K. C. 1998. End-Effectors for Tomato Harvesting Robot. *Artif. Intell. Rev.*, **12:** 11-25.
20. Nikbakht, A. M., Tavakkoli, H. T., Malekfar, R. and Gobadian, B. 2011. Nondestructive Determination of Tomato Fruit Quality Parameters Using Raman Spectroscopy. *J. Agr. Sci. Tech.*, **13:** 517-526.
21. Peña, C., Riaño, C. and Moreno, G. 2018. A Teleoperated Agricultural Robot for Structured Environments. *J. Eng. Sci. Technol. Rev.*, **11**.
22. Silva, F. M., Lichtenstein, G. and Alseekh, S. 2017. The Genetic Architecture of Photosynthesis and Plant Growth-Related Traits in Tomato. *Plant Cell Environ.*, **41:** 327-341.
23. Sabanci, K. and Aydin, C. 2018. Smart Robotic Weed Control System for Sugar Beet. *J. Agr. Sci. Tech.*, **19:** 73-83.
24. Soni, D. P., Ranjana, M. and Gokul, N. A. 2010. Autonomous Arecanut Tree Climbing and Pruning Robot. *International Conference on Emerging Trends in Robotics & Communication Technologies*, 3 December 2010, Chennai, India, IEEE.
25. Tanigaki, K., Fujiura, T. and Akase, A. 2008. Cherry-Harvesting Robot. *Comput. Electron. Agr.*, **63:** 65-72.
26. Ueki, S., Kawasaki, H. and Ishigure, Y. 2011. Development and Experimental Study of a Novel Pruning Robot. *Artif. Life Robot.*, **16:** 86-89.
27. Vasconez, J. P., Kantor, G. A. and Cheein, F. A. A. 2019. Human–Robot Interaction in Agriculture: A Survey and Current Challenges. *Biosyst. Eng.*, **179:** 35-48.
28. Zhu, H., Gu, S. and He, L. 2018. Transition Analysis and Its Application to Global Path Determination for a Biped Climbing Robot. *Appl. Sci-Basel*, **8:** 122.

تحلیل پویای جلوگیری از موانع برای هرس شاخه های جانبی گوجه فرنگی با بازوی رباتیک

ف. یین، ی. شن، ی. چن، س. ژانگ، و م. وو

چکیده

شاخه های جانبی در گیاه گوجه فرنگی اثر زیادی بر عملکرد و کیفیت میوه دارد و امروزه عملیات هرس اساسا با دست انجام می شود که کار زیاد همراه با ریسک است. هدف این پژوهش کار با گوجه فرنگی ایستاده (elevated tomato) بود و با شش درجه آزادی**P-R-R-R-R-R** یک دستگاه بازوی رباتیک برای هرس شاخه های جانبی گوجه فرنگی در محیطی دارای موانع پیشنهاد شد. برای

[DOR: 20.1001.1.16807073.2021.23.1.16.9]

تکمیل شبیه سازی پویا (dynamic simulation) از بازوی رباتیک در محیط دارای موانع، از ADAMS استفاده شد. نتایج شبیه سازی، منحنی های سرعت زاویه ای و شتاب زاویه ای هر مفصل را نشان داد. یک روش برنامه ریزی مسیر حرکت شامل ترکیبی از فضای دکارتی و فضای مشترک پیشنهاد شد تا به طور مطمئنی از برخورد بازوی رباتیک با موانع درحین عمل جلوگیری شده و اثر آن به طور موثری کم شود.

[DOR: 20.1001.1.16807073.2021.23.1.16.9]